Proceedings of the IASS 2024 Symposium
Redefining the Art of Structural Design
August 26-30, 2024, Zurich Switzerland
Philippe Block, Giulia Boller, Catherine DeWolf,
Jacqueline Pauli, Walter Kaufmann (eds.)

Research of lateral impact resistance and axial residual axial bearing capacity of high-strength circular steel tube

Ximei Zhai*, Kaiyun Yang

*Key Lab of Structures Dynamic Behavior and Control of the Ministry of Education, Harbin Institute of Technology, Harbin 150090, China
*Key Lab of Smart Prevention and Mitigation of Civil Engineering Disasters of the Ministry of Industry and Information Technology, Harbin Institute of Technology, Harbin,
150090, China
Email: xmzhai@hit.edu.cn

Abstract

Circular steel tubes are known as one of the most important components in the field of construction engineering, especially in large-span spatial structures, by virtue of their excellent performance. At present, with the frequent occurrence of accidental loads such as terrorist attacks and object impacts on buildings, how to predict and improve the impact resistance of circular steel tubes is known as the current research hotspot. In this paper, an experimental study on the residual stable bearing capacity of the high-strength steel circular tube with impact damage after lateral impact is carried out by means of an axial loading device, and the load-deformation curve, residual stable bearing capacity and deformation characteristics of the member are obtained. The influence degree and law of the specimen slenderness ratio, impact energy and other parameters on the residual stability of the specimen are analyzed, the instability mode of the specimen is defined and classified, and the stable bearing capacity is compared with that of the specimen without lateral impact. The ANSYS finite element (FE) analysis platform was utilized to establish a FE analysis model for the residual stability performance of high-strength steel components, followed by numerical simulations to further conduct parameter analysis.

Keywords: impact, high-strength steel, residual axial bearing capacity, tube, stable bearing capacity

1. Introduction

High-strength steel, renowned for its superior strength and stiffness compared to conventional steel materials, not only offers inherent advantages but also addresses the evolving demands of steel structure construction, particularly for larger spans and greater heights. Serving as primary load-bearing members in steel structures, high-strength steel components face more severe safety issues after unexpected disasters, such as vehicular collisions or construction mishaps, which can result in localized damage or even structural collapse. Lateral impact loads typically exert forces perpendicular or at certain angles to the structural length, resulting in characteristics such as the local depression at the impact position and the overall deformation of the component, these damages will seriously affect the axial bearing capacity of the component. Therefore, given the contemporary trend in structural engineering towards high strength and the urgent safety requirements for engineering impact defense, conducting systematic experiments and research on the post-impact assessment and residual axial bearing capacity of high-strength steel components is paramount. This is essential to promote the application and development of high-strength steel structures and enhance their impact defense capabilities, thus warranting further in-depth research.

In recent years, the study of residual axial bearing capacity of high-strength circular steel tubes after lateral impact has attracted significant attention from scholars. Scholars such as Wan [1] and Chen [2] have conducted axial compression tests on short columns comprised of Q235-grade circular steel

tubes with an outer diameter of 165mm (slenderness ratio is 4.75), as well as square steel tubes (slenderness ratio is 4.74) respectively, after lateral impact. Their studies explored the influence of impact energy, impact location, and diameter-to-thickness ratio on the residual axial strength of the steel columns. Additionally, they proposed empirical formulas aimed at predicting axial strength. Furthermore, scholars Wang [3] and Gong [4] conducted experiments on the residual axial bearing capacity of H-section steel columns after impact, supplemented by FE analysis. They established functional relationships between residual axial bearing capacity, impact energy, and local deformation of the specimen's post-impact. Additionally, Scholar Li [5] investigated the residual axial bearing capacity of circular tubes after lateral impact and proposed two simplified calculation methods.

Existing research mentioned above on the impact conditions of steel components differs significantly from the actual impact conditions encountered by steel structures and current research mainly focuses on conducting lateral impact tests on specimens horizontally placed on steel platforms. Most of the research has primarily focused on short components, whose lengths do not meet the usage requirements of practical steel structure buildings. In addition, with the widespread application of high-strength steel structures, the response results of high-strength steel components after impact, as well as their axial compression stability performance and residual bearing capacity after impact, are all research hotspots worthy of attention. Hence, this study aims to investigate the residual axial bearing capacity of high-strength circular steel tubes after impact through experimentation and FE numerical simulation.

2. Measurement of deformation results for specimens after impact

2.1. Introduction to impact test

Our research group conducted lateral impact tests on 19 high-strength circular steel tubes in the preliminary stage [6]. The design parameters of the experiment including impact energy ($E_k = 0.5Mv^2$, where M is the mass of the impacting object and v is the impact velocity), diameter-to-thickness ratio (D/T), axial compression ratio (R), slenderness ratio （λ）and hammer head shape, including flat, wedge-shaped and hemispherical hammer head. The impact test setup, depicted in Figure 1, involved the free fall of a hammer along the guide rail direction during the test process, thereby imparting impact loads on the specimen. The high-strength circular steel tubes were arranged transversely, and boundary conditions with fixed ends were established using supporting devices on both sides of the circular tubes. Axial force was applied to the specimen through a jack connected to the flanges at the ends of the specimen. The lateral impact test results of the specimens are shown in Table 1.

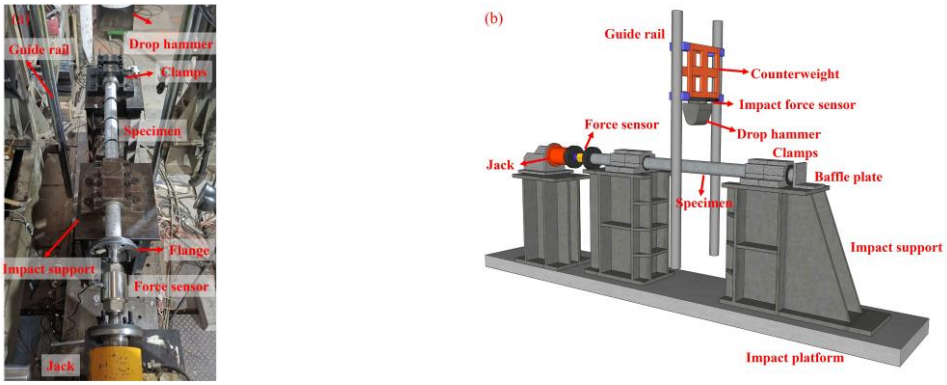

Figure 1: Impact test setup: (a) photo and (b) 3D view.

2.2. Material properties

To obtain the material strength of high-strength steel specimens in this experiment, tensile tests were conducted on 15 specimens. The test results indicate that there is no clear yield point for the A, B, and C types of cross-sections, with an average yield strength of 573 MPa, whereas the D and E types of cross-sections exhibit shorter yield platforms, with an average yield strength of 498 MPa. Here, A to E refer to specimen thicknesses ranging from 2 to 6 mm. The stress-strain curves and mechanical performance parameters of the two types of high-strength steel are shown in Figure 2.

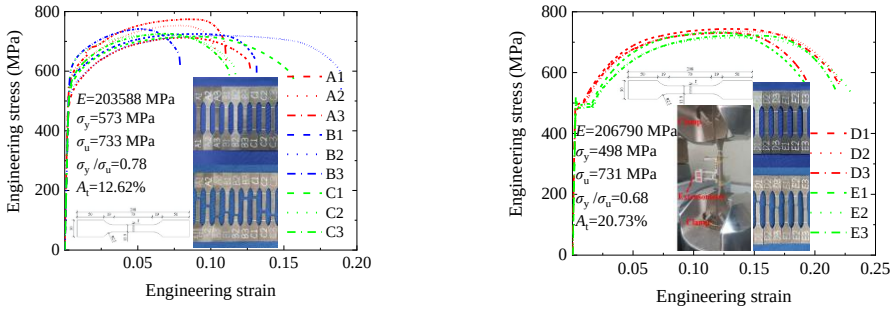

Figure 2: Stress-strain curves of high-strength steel

2.3 Measurement of deformation results after impact

Prior to conducting the residual axial load capacity tests on the 19 impacted specimens, detailed measurements were made of the overall deformation after impact and local indentation deformation at the impact location of these specimens. Using a fully automated laser rangefinder, the local indentation deformation value (δ_D) at the impacted region of the specimen after impact, and the overall deformation value (ω) induced by the impact were measured. The measurement setup, illustrated in Figure 3, utilizes a programmable controller to control a multi-channel data acquisition system, enabling measurements through horizontal movement along the track. The measurement results are presented in Table 1. Two additional specimens, D-E0-R0-1 and D-E0-R0-1 were added at the end of Table 1 for comparison with the axial compression bearing capacity of specimens subject to impact.

Figure 3 fully automated laser rangefinder

Table 1: Specimen geometric parameters and test results.

Specimens	Geometric parameter				Lateral impact test				Axial compression test		
	L/mm	D/mm	T/mm	λ	ω/mm	δ_D/mm	E_k/kJ	R	P_u/kN	ω*/mm	δ_D*/mm
A-E3.4-R0	904	88.93	6.55	15.40	10.912	24.261	3.4	0	823	30.94	37.00
A-E3.4-R1-1	906	88.68	6.48	15.44	12.602	26.582	3.4	-0.2	772	28.61	37.00
A-E3.4-R1-2	905	88.79	6.46	15.41	12.121	25.978	3.4	-0.2	810	24.42	35.00
A-E16-R1	905	88.91	6.67	15.43	60.000	87.070	16	-0.2	460	39.25	46.00
A-E17-R1	905	89.15	6.55	15.36	58.500	92.230	17	-0.2	440	31.25	50.00
A-E5.3-R1	904	89.12	6.55	15.37	22.912	36.261	5.3	-0.2	689	35.80	43.00
A-E14-R1	905	89.00	6.56	15.39	49.100	80.160	14	-0.2	515	35.00	39.13
A-E14-R2	905	89.00	6.41	15.36	50.500	79.690	14	-0.3	490	38.27	50.00
A-E14-R3	904	89.57	6.73	15.31	41.740	63.000	14	0.2	545	34.67	57.00
A-E14-R0	903	88.90	6.60	15.42	47.500	76.430	14	0	521	35.61	41.00
B-E3.4-R0	902	88.98	9.21	15.85	8.490	14.650	3.4	0	1220	32.35	40.00
B-E14-R1	904	89.30	8.69	15.70	32.800	50.390	14	-0.2	900	30.96	35.00
C-E3.4-R0	902	89.29	9.60	15.86	8.480	15.560	3.4	0	1206	41.80	49.00
C-E14-R1	906	88.51	9.60	16.00	32.640	48.760	14	-0.2	922	34.72	42.00
D-E5.3-R1-F	908	102.07	10.20	13.77	7.488	8.020	5.3	-0.2	1673	44.61	43.00
D-E5.3-R1-H	906	102.44	10.14	13.70	8.017	15.021	5.3	-0.2	1610	41.33	46.00
F-E30-R0	906	76.14	8.91	18.78	101.000	128.90	30	0	345	33.27	38.00
F-E30-R1	903	76.24	8.52	18.65	137.000	158.50	30	-0.2	330	29.28	37.00
F-E30-R2	905	76.52	8.91	18.66	115.000	144.31	30	-0.3	330	28.61	36.00
D-E0-R0-1	905	102.27	10.25	13.75	0	0	0	0	1920	/	/
D-E0-R0-2	905	102.44	10.33	13.73	0	0	0	0	1948	/	/

Note: $R = N/A\sigma_y$ is the axial pressure ratio (N represents axial force, A denotes the cross-sectional area of the specimen, and σ_y is the yield strength of the material), when R is positive it indicates the specimen is under tension and when R is negative it identifies the specimen is under compression.

The specimens are named based on three parameters: cross-sectional dimensions, impact energy, and axial compression ratio. For example, in the designation A-E3.3-R0, “A” represents the cross-sectional dimensions (the specimens has five different cross-sectional dimensions corresponding to A~F), “E3.3” indicates an impact energy of 3.3 kJ, and “R0” signifies an axial compression ratio of 0. Furthermore, for specimens numbered as A-E3.4-R1-1 and A-E3.4-R1-2, the final “1” and “2” indicate that these specimens are duplicates. For specimens numbered as D-E5.3-R1-F and D-E5.3-R1-H, “F” and “H” represent the types of hammers used to impact these specimens, where “F” denotes a flat hammer head and 'H' denotes a hemispherical hammer head. For other specimens not specified with a hammer head type, wedge-shaped hammer heads were used for impact testing.

3. Axial compression test of specimens after lateral impact

3.1 Test setup and measurement system

The experiments were conducted using an electro-hydraulic servo press, as depicted in Figure 4. To ensure consistency in the specimens' end conditions between the impact test and the axial compression test, both ends were rigidly supported. This was achieved by pre-drilling four bolt holes on each side of the specimen's end plates. Bolts were then used to connect the end plates of the specimen to the electro-hydraulic servo press.

During the experiment, the overall deformation（ω*） of the specimen was measured using a linear displacement meter，simultaneously using a combination of laser rangefinder and MS60 total station to measure the local indentation deformation（δ_D*) of the specimen. The schematic diagram of the measurement device is shown in the Figure 5.

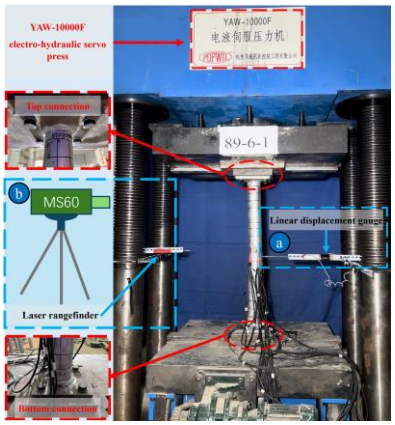

Figure 4 Electro-hydraulic servo press

Figure 5 Diagram of measurement device

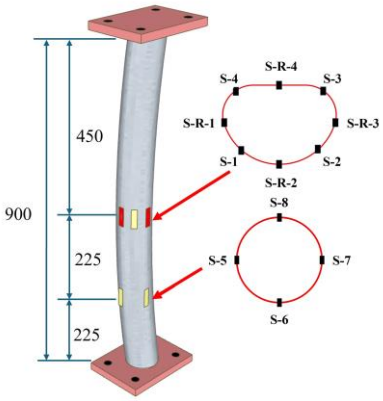

Figure 6 Layout plan of strain gauges

As shown in Figure 6, during the axial compressive experiment, strain gauges (S-1~S-8 and S-R-1~S-R-4), pasted along the length direction of the specimens, were used to measure the strain situation at the 1/2 and 1/4 span of the specimens. The strain gauge S-R-4 is located at the position of the local indentation caused by the impact.

3.2 Experimental results and analysis

3.2.1 Loading process and failure mode

During the experimental process, the electro-hydraulic servo press adopted a displacement control mode with a loading speed of 0.3mm/min. Loading continued until the load decreased to 85% of the stable bearing capacity peak. The peak load (P_u) of the specimens obtained from the electro-hydraulic servo press, as well as the displacements measured by the measurement device for overall deformation （ω*） and local indentation deformation（δ_D*), were all recorded in Table 1.

Analyze the load-displacement curves of specimens without impact and specimens subject to impact during the loading process. (as shown in the figure 7(a)), it was found that specimens without

impact entered the yield stage after the elastic stage and had a clear yield plateau, followed by the strengthening and plastic stages.

The specimens subject to impact exhibited significant differences in the load-displacement curve compared to the specimens without impact due to localized buckling during the axial compression process. For specimens with minor impact, after the elastic stage, their residual axial bearing capacity continues to increase to some extent in the elastic-plastic stage. However, as they enter the plastic stage, their residual axial bearing capacity rapidly decreases. In contrast, as the weak area of the specimen subject to significant impact, the local indentation intensifies the failure of the specimen. the specimen quickly enters a brief elastoplastic stage, with no significant increase in residual axial bearing capacity. Subsequently, they enter the plastic stage, with residual axial bearing capacity decreasing slowly.

Further analysis and research are conducted on the localized buckling of specimens subject to impact under axial compression. For most specimens subjected to significant impact underwent three stages during axial compression, including (1) elastic stage, (2) elastic-plastic stage, and (3) plastic stage, as shown in Figure 7(b).

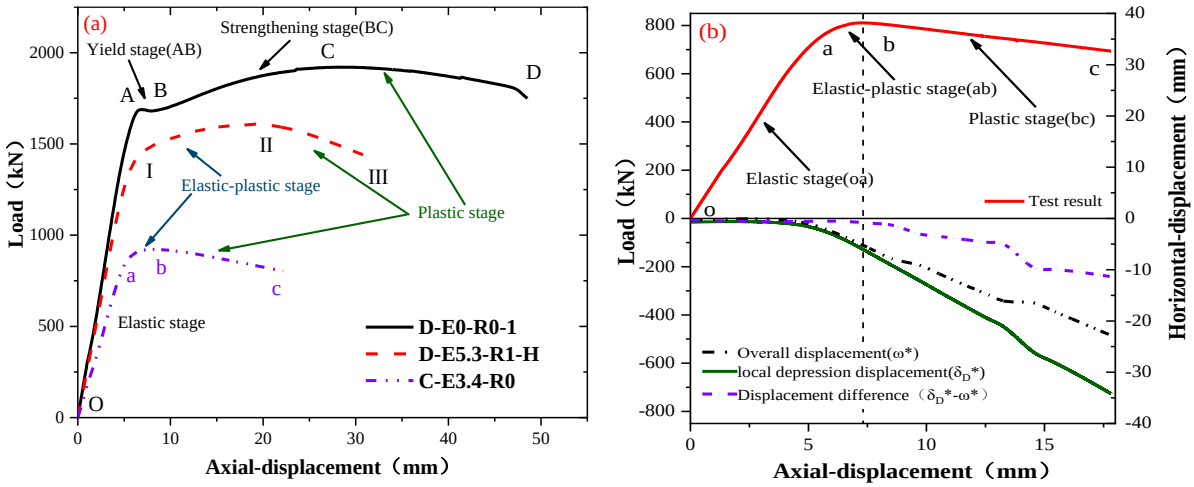

Figure 7 Load process of high-strength circular steel tube

Taking the A-E3.4-R1-2 specimen as an example, the load-displacement curve of the specimen exhibits linear characteristics under lower axial loads. The overall displacement and local indentation displacement of the specimen do not develop significantly until the axial load reaches the peak load, and both begin to gradually increase. When the axial load reaches its peak value, the local indentation displacement of the specimen begins to further develop relative to its overall displacement, indicating that local buckling is one of the main reasons for the reduction of the residual axial bearing capacity of the specimen. The specimen then enters a brief elastic-plastic stage, with a peak load force of approximately 780kN. As the axial displacement further increases, the specimen enters the plastic stage, and its local indentation displacement and overall displacement further increase. At the same time, the displacement difference also gradually increases, indicating that the impacted position of the specimen, as the weak area of the specimen, undergoes significant deformation during the entire axial compression process with impact.

An analysis was conducted on the failure modes of specimens under different impact energies, axial compression ratios, diameter to thickness ratios, and hammer head shapes. Local indentation in the specimens further developed during axial compression tests, serving as weak areas during the axial compression process, greatly reducing the residual axial bearing capacity of the specimens. Summarizing the experimental phenomena, it can be concluded that all specimens subjected to impact exhibit a combined failure mode of local buckling and overall bending instability during axial compression, as shown in Figure 8.

Figure 8 Failure model

3.2.2 Load-strain response

Further analysis and research are conducted on the load-strain behavior at the mid-span of specimens with different degrees of impact damage. Taking specimens, A-E14-R1 and C-E3.4-R0 as examples, the load-strain curves are shown in Figure 9. The arrangement scheme of strain gauges for the mid-span section of the specimen is shown in Figure 6. The vertical axis in the figure represents the axial compressive load, the horizontal axis represents the longitudinal strain of the specimen, where negative values represent compressive strain and positive values represent tensile strain. In the elastic stage, the strain increases linearly with the load, but the increase is relatively small; In the elastic-plastic and plastic stages, the strain significantly increases with the increase of load.

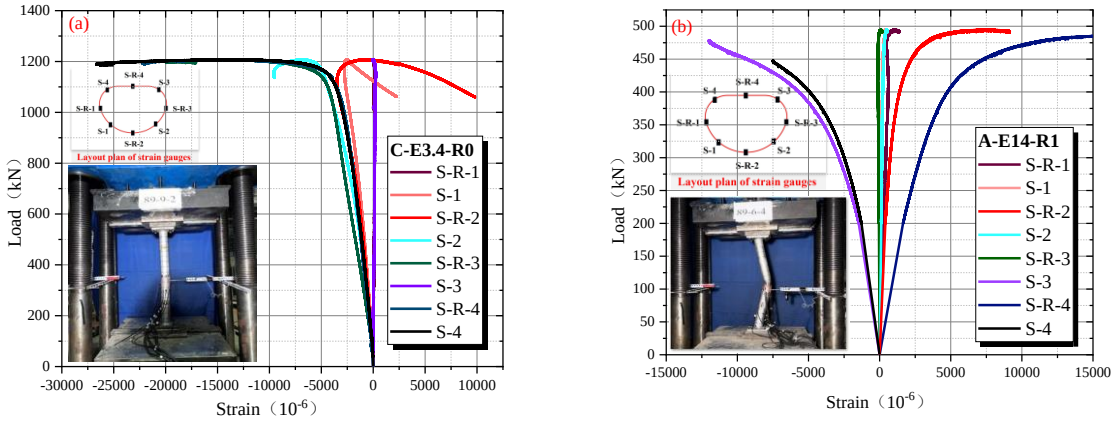

Figure 9 Load-strain curve

For specimen (C-E3400-R0) subject to minor impact, as depicted in the figure9(a), it transitions from initially being under full-section compression during loading to experiencing tension at the opposite face of the impact location (S-R-2), while facing compression at the impact location itself (S-R-5). As the degree of impact damage on the specimen increases, as in the case of specimen A-E14000-R1 (as depicted in the figure9(b)), tension begins to occur at the opposite face of the impact location (S-R-2) and at the impact location itself (S-R-5) during the initial loading stage. The tensile strain at the impact location (S-R-5) relative to the opposite face of the impact location (S-R-2) further develops as the degree of impact damage increases. The position of the maximum tensile strain shifts from the opposite side of the impact position to the impact position. This is because during the axial compression process, the local indentation of the specimen will further develop compared to its overall deformation, leading to a change in the maximum tensile strain value.

4. FE modeling and Verification.

This section is based on ANSYS/LS-DYNA FE software to establish FE simulation of high-strength circular steel tubes under axial load with impact. The FE simulation is divided into two parts, including (1) Lateral impact FE simulation of high-strength circular steel tubes, and (2) Axial compression simulation of high-strength circular steel tubes with impact. Based on the FE model after lateral impact, ANSYS FE software was used to simulate axial compression using a complete restart technique. （The complete restart technique can handle multiple load conditions sequentially for a FE model. This technique retains the load response of the FE model after lateral impact (including residual deformation, residual stress, etc.), and considers the load response of the previous FE model when starting the simulation of axial compression, thereby enhancing the rationality and accuracy of finite element analysis.）

To enhance the accuracy of numerical simulation results regarding axial compression simulation of high-strength circular steel tubes with impact, it is necessary for the overall deformation values and the local indentation deformation values of the FE model of the circular steel tube subjected to lateral impact to closely match the measured overall deformation（ω*） and the local indentation deformation（δ_D*) values ,as shown in Table 1, thus achieving the goal of precise modeling.

By modifying the K file for simulating the lateral impact of high-strength circular steel tubes and inputting the keyword *INTERFACE_SPRINGBACK_LSDY, the residual deformation and residual stress distribution of the FE model after lateral impact can be exported as a dynain file. This dynain file can then be used as the FE model for subsequent axial compression simulation analysis. The high-strength circular steel tube uses shell elements (SHELL163) and is refined within a 150mm range to the left and right of the center of the impact position. The mesh size in the refined area is 2mm, while the non-refined area on the tube has a mesh size of 10mm. Other parts are modeled using solid elements (SOLID164), with an approximate mesh size of 15mm. By modifying the K file for simulating the lateral impact of high-strength circular steel, irrelevant elements for the axial compression simulation are removed, leaving only the two side plates from the lateral impact simulation, along with the removal of redundant constraint conditions. The exported dynain file from the lateral impact simulation is imported into the K file to obtain the FE for the axial compression simulation. The material model for this FE model remains consistent with the previous FE simulation. The imported FE model needs to redefine the contact between elements. Using the keyword *BOUNDARY_SPC_SET, symmetrical constraints are applied to the high-strength circular steel tube with impact, ensuring that the constrained half-model experiences the same force state as the full model. In the experiment, the side plates are welded to the high-strength circular steel tube to ensure that the tube does not crack at the weld during the axial compression test. In the FE simulation, the contact between the two is set as *CONTACT_TIED_NODES_TO_SURFACE_OFFSET, which ensures a firm constraint between the side plates and the high-strength circular steel tube. A uniform loading curve is defined using the keyword *DEFINE_CURVE, and the loading velocity is assigned to one end plate using the keyword *BOUNDARY_PRESCRIBED_MOTION_RIGID, mimicking the experimental process of uniformly displacing the pressure machine. Horizontal displacement and rotational degrees of freedom for the two side plates are constrained to ensure fixed support at both ends during the axial compression test.

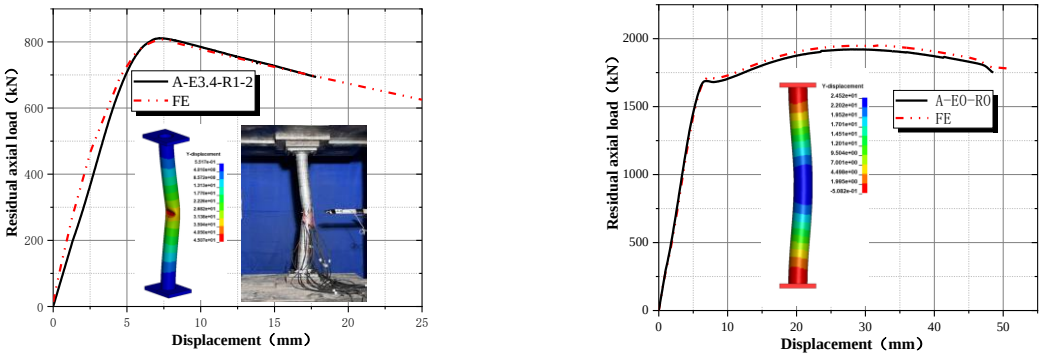

Figure 10 FE Verification

Taking specimens, A-E3.4-R1-2 and D-E0-R0-1 as examples, Figure 10 compares the load-displacement curves obtained from the specimens with those obtained from FE simulation. The buckling load and experimental error of FE numerical simulation are both within 10%, indicating that the FE numerical simulation results are reliable.

5 Analysis of factors affecting residual axial bearing capacity

This section mainly discusses the effects of impact energy, diameter to thickness ratio, axial compression ratio, and hammer head shape on the residual axial bearing capacity of high-strength circular steel tubes with impact. By using FE numerical simulations to supplement the load-displacement curves of undamaged specimens from impact with different cross-sections that were missing in the experiments, further analysis can be conducted on the influence of the above parameters on the residual axial bearing capacity of the specimens.

5.1 Effect of impact energy

The residual axial load-displacement curves of specimens under different impact energies are shown in Figure 11. From the figure, as the impact energy increases, both the residual axial bearing capacity and stiffness of the specimen decrease simultaneously. For example, when the impact energy increases from 3.4kJ to 17kJ, the residual axial bearing capacity of the specimen decreases by 20.4% to 56.22%. The impact energy has a significant impact on the residual axial bearing capacity of the specimen. With the increase of the impact energy, the local and global impact deformation response of the specimen increases, and the second-order effect becomes more significant. At the same time, from the stiffness of the specimen, when the impact energy is small, such as when the impact energy is from 3.4kJ to 5.3kJ, the impact energy weakens the test stiffness slightly. However, as the impact energy gradually increases, its impact on the specimen stiffness also intensifies.

5.2 Effect of diameter-thickness ratio

The residual axial load-displacement curves of specimens under different diameter to thickness ratios are shown in Figure 12. The diameter to thickness ratio of the specimen increased from 9.3 to 13.58, and the residual axial bearing capacity of the specimen decreased by 43.38% to 48.5%. At the same time, the initial stiffness of the specimen also significantly decreased with the increase of the diameter to thickness ratio. Specimens with a large diameter to thickness ratio produce significant residual deformation due to lateral impact, and the second-order effect is significant. Their residual axial bearing capacity and overall stiffness loss are relatively large, but specimens with a small diameter to thickness ratio have better resistance to deformation caused by impact, and their residual axial bearing capacity and overall stiffness loss are relatively small.

5.3 Effect of axial compression ratios

The Residual axial load-displacement curves of specimens under different axial pressure ratios are shown in Figure 13. It can be observed that the residual axial bearing capacity of specimens under different axial pressure ratios decreased by 45.76% to 50.85% at the same impact energy level. Specifically, at the same level of preloaded axial force, the residual axial bearing capacity of specimens subjected to axial tension (R=0.2) was only increased by 52 kN (5.09%) compared to specimens subjected to axial compression (R=-0.2), indicating that the influence of axial compression ratio on the residual axial bearing capacity of specimens is not significant. Furthermore, after lateral impact, the residual deformation of specimens subjected to axial tension (R=0.2) (ω=41.740mm, δ_D =63.00mm) was less than that of specimens subjected to axial compression (R=-0.2) (ω=50.50mm, δ_D =79.69mm), suggesting that preloading axial tension before lateral impact can to some extent reduce the weakening effect of impact on the residual axial bearing capacity of specimens.

5.4 Effect of shape of the hammerhead

The Residual axial load-displacement curves of specimens under different hammer heads are shown in Figure 14. It can be observed that there are significant differences between the specimens with impact and those without impact during axial compression. During axial compression, the specimens

without impact exhibit a distinct yield stage and strengthening stage, with better plasticity. The residual deformation of specimen D-E5300-R1-F under the flat hammer head is minimal, with only a 12.4% decrease in residual axial bearing capacity. Additionally, its behavior during axial compression is similar to that of specimens without impact. In contrast, the residual axial bearing capacity of specimen D-E5300-R1-H under the hemispherical hammer head decreased by 16.7%, and it failed prematurely after experiencing significant plastic deformation. This indicates that different indentation types after lateral impact also have a significant impact on the residual axial bearing capacity of specimens.

5.5 Effect of slenderness ratio

Through FE numerical simulation, the influence of different slenderness ratios on the residual axial bearing capacity of high-strength circular steel tubes was investigated, while keeping the specimen cross-sectional dimensions and other parameters unchanged, and only varying the specimen length (with specimen lengths of L=1200mm (λ=20) and L=1500mm (λ=25) for the FE model of circular steel tubes). It was observed, as illustrated in the figure 15, that the residual axial bearing capacity of high-strength circular steel tubes decreases significantly with an increase in the slenderness ratio. Specifically, when the slenderness ratio of the specimen increased from 15 to 25, the residual axial bearing capacity decreased by 46.4% to 58.7%. Moreover, specimens with a slenderness ratio of 25 exhibited global deformation and local deformation at mid-span following lateral impact that were 84.8% and 36.6% greater, respectively, than those in specimens with a slenderness ratio of 15. Furthermore, this observation suggests that high-strength circular steel tubes with larger slenderness ratios experience a notable increase in second-order effects during axial compression, resulting in a significant reduction in their residual axial bearing capacity.

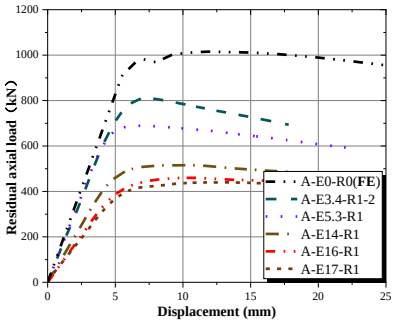

Figure 11 Residual axial load-displacement curve of specimens under different impact energies

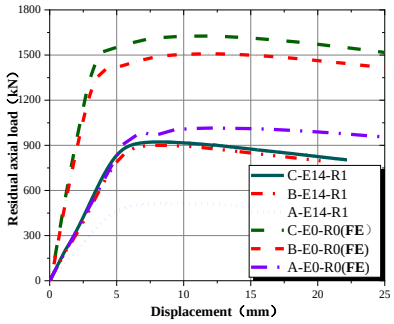

Figure 12 Residual axial load-displacement curve of specimens under different diameter to thickness ratios

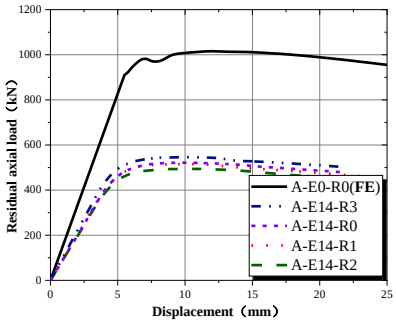

Figure 13 Residual axial load-displacement curve of specimens under different axial compression ratios

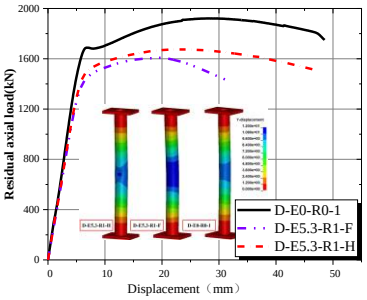

Figure 14 Residual axial load-displacement curve of specimens under different hammer heads

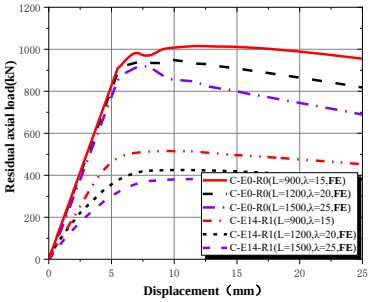

Figure 15 Residual axial load-displacement curve of specimens under different slenderness ratio

6. Conclusions

(1) Under the same impact energy, as the diameter to thickness ratio of the specimens increased from 9.3 to 13.58, the residual axial bearing capacity of the specimens decreased by 43.38% to 48.5%.

The residual deformation generated by lateral impact on high-strength circular steel tubes increases, and their resistance to impact decreases.

(2) The residual axial bearing capacity of specimens is negatively correlated with impact energy and slenderness ratios respectively. When the impact energy increases from 3.4kJ to 17kJ, the residual axial bearing capacity of the specimens decreases by 20.4% to 56.22%. In addition, when the slenderness ratio of the specimens increased from 15 to 25, the residual axial bearing capacity decreased by 46.4% to 58.7%.

(3) The residual axial bearing capacity of specimens under different axial pressure ratios decreased by 45.76% to 50.85% at the same impact energy level, suggesting that preloading axial tension before lateral impact can to some extent reduce the weakening effect of impact on the residual axial bearing capacity of specimens.

(4) The load-displacement curves of high-strength circular steel tubes under different hammerheads vary greatly, with flat hammerheads having a larger contact area with the specimen, which weakens the residual axial bearing capacity of the specimens to a lesser extent. The load-displacement curve of the specimens without impact has obvious yield stage and strengthening stage, while the specimens with impact does not exhibit these stages due to residual deformation.

(5) As the degree of impact damage increases in high-strength circular steel tubes, the second-order effect becomes more pronounced during axial compression, leading to a decrease in their initial stiffness.

Acknowledgements

The research presented in this paper is financially supported by the National Natural Science Foundation of China (Grant No: 52278168).

References

[1] Wan Jun, Chen Yu, Wang Kai, Han Shaohua. Residual strength of CHS short steel columns after lateral impact[J]. 2017,118: 23-36.

[2] Chen Yu, Wan Jun, Wang Kai, Han Shaohua. Residual axial bearing capacity of square steel tubes after lateral impact[J]. Journal of Constructional Steel Research, 2017, 137: 325-341.

[3] Wang, Experimental study on vertical residual bearing capacity of H-shaped steel column with local buckling deformation[J], Structures, 2014, 44(21):17-22

[4] Gong, Dynamic Response and Residual Structural Capacity Study of H-Shaped Steel with Different Width-Thickness Ratio of the Plate under Impact Load[D]. Taiyuan: Taiyuan University of Technology , 2018.

[5] Ruoxuan Li, Daisuke Yanagihara, Takao Yoshikawa, Axial compressive residual ultimate strength of circular tube after lateral collision[J]. International Journal of Naval Architecture and Ocean Engineering, 2019, 11: 396-408.

[6] Cui G M, Zhai X M, Meng L Z. Behavior of axially loaded high-strength steel circular hollow section tubes under low velocity lateral impact [J]. Thin-Walled Structures, 2023, 185: 110595.